CAAP Annual Report

Date of Report: *10/09/2025*

Prepared for: *U.S. DOT Pipeline and Hazardous Materials Safety Administration*

Annual Period: **From** *(09, 29, 2024)* **to** *(09, 29, 2025)*

Contract Number: *693JK32350002CAAP*

Project Title: *A Novel Reliability-Based Approach for Assessing Pipeline Cathodic Protection (CP) Systems in External Corrosion Management*

Prepared by: *Qindan Huang, Qixin Zhou, Gabriel Langlois-Rahme*

Contact Info.: *Qindan.huang@marquette.edu, 414-288-6670*

qzhou@uakron.edu, 330-972-7159

gabriel@infermodel.com, 514-709-6779

Table of Contents

Section A: Business and Activities

(a) Contract Activities

- Contract Modifications: NA
- Educational Activities:
  - Student mentoring:

    Emad Farahani, a Ph.D. student in Civil, Construction and Environmental Engineering at Marquette University has been working on the project since the project was launched.

    Yuhan Su, a Ph.D. student in Chemical Engineering at The University of Akron is working on the project starting the 3rd quarter of this project.

    Abby Murray, an undergraduate student in Corrosion Engineering at The University of Akron has worked on the project from the 3rd quarter to the 7th quarter of this project.

  - Student internship: NA

  - Educational activities:

    The graduate student, Emad Farahani, participated 3-Minute Thesis competition at Marquette University and was listed as one of the top 10.

    The co-PI (Dr. Zhou) introduced the concept of cathodic protection in the undergraduate course—Introduction to Corrosion Science and Engineering at The University of Akron.

  - Career employed: NA

  - Others: NA

- Dissemination of Project Outcomes:
  Oral presentation: "A Probabilistic Approach to Predicting External Corrosion Density in Buried Steel Transmission Pipelines Using MFL ILI Data", *AMPP*, Nashville, TN, 2025.

- Citations of The Publications: NA
- Others: NA

(b) Financial Summary

- Federal Cost Activities:
  - PI/Co-PIs/students involvement:

PI (Dr. Huang) and one graduate student (Emad Farahani) from Marquette University were charged from this project for the salary during this reporting period.

- Materials purchased/travel/contractual (consultants/subcontractors):

  Subcontractor, University of Akron has worked on Task 3.

  InferModel as the hired consultant has helped on Task 2 (Data collection and analysis).

- Cost Share Activities:

  - Cost share contribution: The cost share of Dr. Huang's academic salary from Marquette University has been charged as planned.

(c) Project Schedule Update

- Project Schedule:
  Table A shows the original proposed schedule.

Table A. Original schedule and milestones of proposed tasks

Tasks	Year 1				Year 2				Year 3			
Task 1. Literature Review												
Task 2. Data collection and analysis												
Task 3. Stray current corrosion												
Task 4. Probabilistic defect growth modeling												
Task 5. Time-dependent reliability												
Task 6. CP performance and management												
Final Report												

- Corrective Actions:
  Table B shows the updated research tasks. Task 1 took more time than originally planned, which was necessary to make sure the research team thoroughly understands the mechanics of cathodic protection systems, the current practice on external corrosion management, and state-of-art research that related to the project. Task 2 took more than the original planned as well due to the complexity and large size of the data types and the needed various data validations. Task 3 started a quarter later than the original plan. To improve model accuracy, various modeling approaches have been explored for Task 4. Tasks 5 and 6 will formally start in Year 3, as the majority effort has been put in Task 4 in Year 2.

Table B. Updated schedule and milestones of proposed tasks

Tasks	Year 1				Year 2				Year 3			
Task 1. Literature Review												
Task 2. Data collection and analysis												
Task 3. Stray current corrosion												
Task 4. Probabilistic defect growth modeling												
Task 5. Time-dependent reliability												

Task 6. CP performance and management												
Final Report												

(d) Status Update of the 8th Quarter Technical Activities

- Task 3: Stray current corrosion (in progress)
  During the past quarter, the students conducted DC interference testing for X60 samples. The corrosion was measured by electrochemical testing and weight loss measurement.

- Task 4: Probabilistic defect growth modeling (in progress)

  This task started in the 5th quarter. So far, we have conducted model development for corrosion defect occurrence, corrosion density, and area/volume growth.

- Task 5: Time-dependent reliability analysis

  This task will start in the 9th quarter.

- Task 6: CP performance and management

  This task will start in the 9th quarter.

Section B: Detailed Technical Results in the Report Period

1. Background and Objectives in the 2nd Annual Report Period

1.1. Background

The purpose of this research project is to develop a novel reliability-based approach for assessing pipeline cathodic protection systems for the prevention of external corrosion. To develop a novel approach, a thorough literature review and data engineering initiative is required.

Existing structural reliability frameworks on the corrosion response of inline inspections (ILI) detected anomalies have been reviewed. These frameworks apply effective area burst pressure estimations on corrosion clusters while explicitly accounting for material uncertainties, sizing uncertainties, model uncertainties and growth uncertainties. This leads to a burst pressure distribution that can be compared against an operating pressure distribution towards assessing pipeline reliability. These reliability assessments provide informative information around excavation decisions, re-inspection intervals, and can perhaps provide additional insights on decision making around corrosion prevention, especially around impressed current cathodic protection systems. These decisions can involve budget allocation around the replacement of anode beds, increasing rectifier currents, or performing Closed Interval Surveys (CIS) for more granular information around the effectiveness of cathodic protection systems.

1.2. Objectives in the 2nd Annual Report Period

During this reporting period, there are three main objectives:

- Complete collecting and analyzing relevant data of transmission pipelines from industry partners
- Review the past lab testing of samples under CP with DC inference
- Model development of corrosion behavior using ILI data

2. Task 2 Data Collection and Analysis

All digitized closed interval survey (CIS) information has been integrated into the project dataset. This involved extracting survey information using regular expressions from 500 survey files, and correlating them to data quality excel sheets. From there, the spatial coordinates of the CIS were used to correlate measurements to the location on all applicable historical ILI inspections. Additionally, corrosion density measurements and maximum depth and growth rates have been correlated to CIS measurements for each ILI period.

Climate data from the National Oceanic and Atmospheric Administration (NOAA) for the years 2020 to 2023 has been correlated with each pipeline joint in this study, wherever available. Two distinct approaches were employed:

- **Standard weather station correlation**
  Pipeline joints were matched to the nearest weather station.
- **High-quality weather station correlation**
  Pipeline joints were matched to the nearest high-quality USW weather stations (e.g., airports, large facilities) that provided more variables and consistent daily measurements.

A total of 92 weather stations, including 22 high-quality stations, were utilized in this study. Using the collected data, the following environmental variables were derived for both approaches: Freeze-Thaw Cycle, Time of Wetness, Wet-Dry Cycle, Precipitation Over 1 Inch, Snow Days, Atmospheric Relative Humidity.

Historical data on rectifier circuit resistances and resistivities were analyzed to develop a seasonal model error for all rectifiers used in this study. A normal distribution was identified as the best fit for the data, based on the lowest Akaike Information Criterion (AIC). Furthermore, rectifier circuit resistivities were compared with gSSURGO soil resistivities measured during the same year at varying distances from the rectifier locations. An order-of-magnitude comparison of soil resistivity data from different sources was performed using the Root Mean Square Logarithmic Error (RMSLE) to evaluate field versus estimated results.

Finally, *inferModel* has further augmented the box-to-box matching used in this study, with an improved feature matching algorithm compared to the feature matching software used by the industry partner.

3. Task 3 Corrosion Behavior Under Stray Current Interference

3.1. Background and Objectives in the 2nd Annual Report Period

The influence of AC interference is complex under different CP conditions and surrounding environments. The research team has obtained a good understanding of the key influencing factors in AC corrosion that contribute to CP effectiveness: AC current density, CP current density, and CP potential for a given metal in a soil environment, through a recently completed PHMSA CAAP project. In the meantime, it is known that DC interference cannot be ignored for pipelines under cathodic protection, especially for non-stationary dynamic DC interference. The objective of Task 3 in this reporting period is to design experiments to study metal corrosion under DC interference.

3.2. Research Progress in the 2nd Annual Report Period

a) Experimental design

1) Materials

Metal: API 5L X60 was purchased from the Metal Samples company. Its chemical composition is 0.15% C, 1.15% Mn, 0.009% P, 0.002% S, 0.25% Si, and balanced with Fe. Two types of metal testing coupons were prepared: the mounted coupon and the weight loss coupon.

The mounted metal coupons were used for electrochemical measurements, including potentiostat, galvanostat, potentiodynamic polarization, and electrochemical impedance spectroscopy (EIS). A copper wire was welded to the back of each cut metal sample to serve as the working electrode. Subsequently, the metals were meticulously sealed with epoxy, ensuring no grooves or bubbles at the epoxy/steel interface. To achieve a smooth and uniform surface, the mounted steel surfaces were polished using 240, 400, 600, 800, and 1200 grit sandpapers, resulting in a mirror-like finish free from scratches. The working area of each specimen was maintained at 2 cm^2.

The corrosion coupons, with dimensions of 3" × 0.5" × 0.063", were used for weight loss measurements. Before testing, the specimens underwent a thorough cleaning process using distilled water and acetone to ensure their cleanliness.

Solution: The test solution used in this study was a simulated soil solution consisting of 8.933 g/L KCl (99%), 0.674 g/L Na_2SO_4 (98%), and 5.510 g/L $NaHCO_3$ (100%), with a pH of 8.35 and a conductivity of 18.60 mS/cm. The testing solution was designed considering the major elements in soils and followed previous studies on the simulated solutions. All solutions were prepared from analytic-grade reagents and deionized water. All experiments were conducted at room temperature (~22°C) and open to air.

2) Experimental setup

The schematic diagram of the experimental setup is shown in Figure 1, including the CP protection circuit and DC interference circuit. In the CP protection circuit, CP potential is applied potentiostatically by Gamry Reference600 working station (#1) with a three-electrode system containing the steel specimen as working electrode (WE), a platinum sheet as counter electrode (CE), and a saturated calomel electrode (SCE) as reference electrode (RE). The CP potential for the DC interference study is designed to be -0.775 V vs. SCE and -1.12 V vs. SCE.

In the DC interference circuit, the working station (#2) is used to apply DC interference between the metal specimen and the counter electrode. Various DC currents, i.e., 0.1, 1, 10 A/m^2, are applied by Gamry Reference 600 Chronopotentiometry mode. This design is to investigate the pulse DC interference rather than the stationary DC interference. Traction current can be divided into two parts based on the speed of the metro: variable speed and constant speed. The variable speed scenario occurs when the metro approaches the entrance and exits of a metro station. The constant speed situation refers to when the metro maintains a stable state during uniform operation. In the previous papers, the stationary wave, sinusoidal, triangular, and square forms were studied [1–6]. However, in the real world, the traction current is not symmetrical like studied before.

Thus, Figure 2 shows the schematic representation of the rectangular wave signals considering pulse DC density to simulate the traction current generated by the metro movement in the real world. The variable speed to the whole speed period is planned to be 1:10, 1:2 (5:10), 9:10, 1 (10:10). The variable speed was set as 12s. The durations were set to be 1 and 3 days.

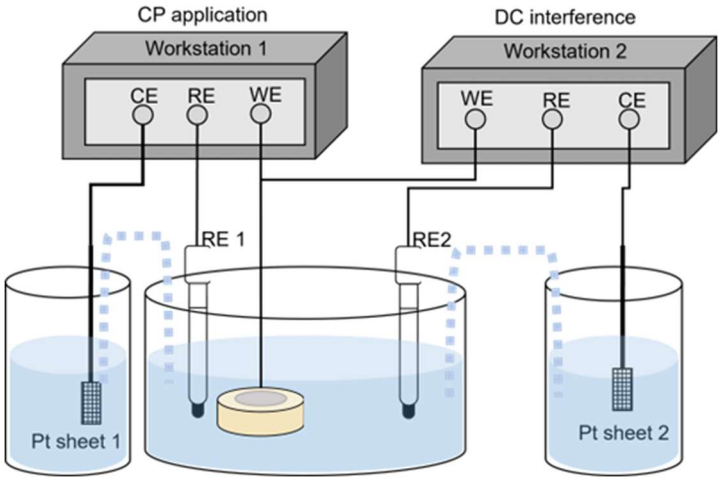

Figure 1. Schematic diagram of the experimental setup of DC interference corrosion of X60 under cathodic protection.

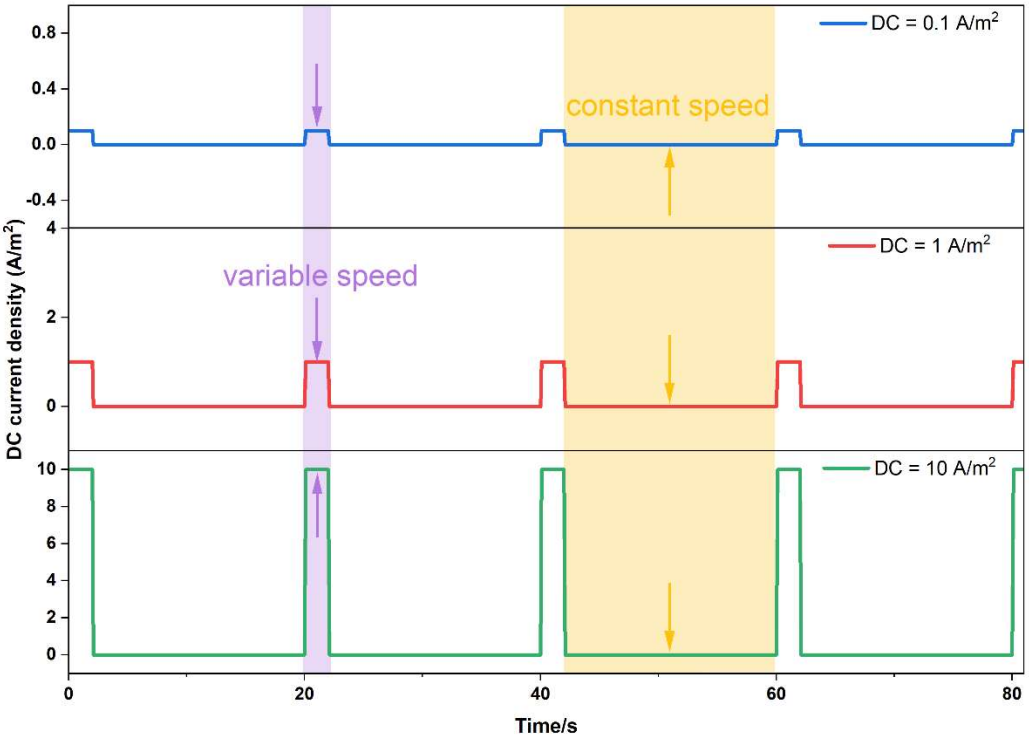

Figure. 2. Schematic representation of different DC current densities with an interference period of 1/10.

3) Characterization methods

In this experiment, Tafel testing and weight loss measurement are scheduled to determine the corrosion rate of X60 under various DC interference and CP potential conditions. Mounted

metal coupons are employed for the Tafel test, and corrosion coupons are used for weight loss measurement. Figure 3 shows the experimental protocol to investigate the DC interference corrosion. The initial pH and the open circuit potential (OCP) of the metal are tested before the application of DC interference and CP potential. Following the predefined time period, EIS, Tafel, and morphology tests are carried out to evaluate corrosion.

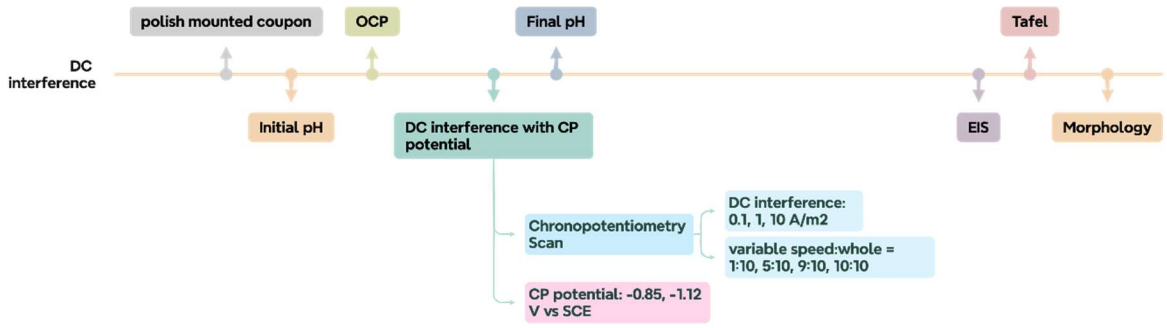

Figure 3. Experimental protocol for the study of DC interference corrosion.

b) Results and Discussion

1) Weight loss of X60 under different DC interference without CP

So far, the DC interference corrosion of X60 steel has been studied at three DC interference levels (0, 0.1, 1, 10 A/m^2), and different interference periods (IP) (0, 1/10, 5/10, 9/10, 1), by weight loss measurement for three days of immersion. Some data points are in progress under the weight loss testing.

Figure 4 shows the corrosion rate of X60 under different DC current densities and interference periods in units of mpy. Their corresponding surface morphology after chemical cleaning is presented in Figure 5. It is observed that the corrosion rate increased with an increase in the interference period. The largest value occurred when the interference period reached 1. Based on the surface morphology, no obvious pitting was observed on the surface. Thus, DC interference resulted in uniform corrosion based on weight loss measurement.

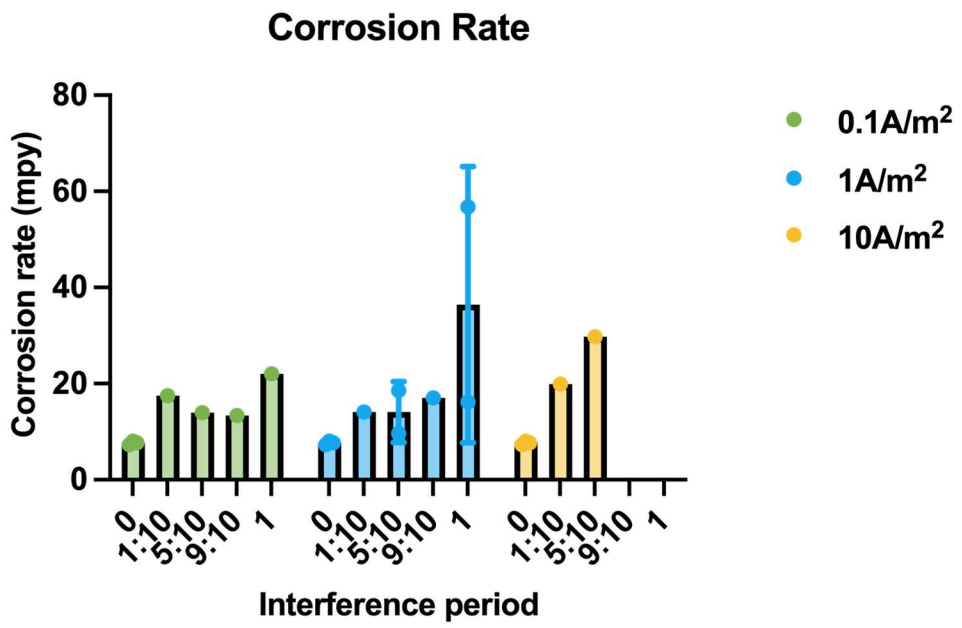

Figure 4. Corrosion rate (mpy) of X60 under different DC current density and interference periods.

Figure 5. Surface morphology of weight loss coupons after chemical cleaning, following ASTM G1 standards.

2) DC potential monitoring and EIS measurement

The DC potential monitoring of X60 steel under DC current density of 0.1 A/m^2 and interference period (IP) of 1/10 is shown in Figure 6a. Curves of rainbow colors correspond to measurements at different time periods (0.5h, 1h, 3h, 6h, 12h, 12.5h, 15h). DC potential is the feedback of the applied DC current density. Due to the interference period, the DC potential has the shape of a peak and valley, corresponding to the feedback of the variable speed and constant speed of the applied DC current during the whole process, respectively. The valley potential gradually shifted negatively from –0.8228 V vs. SCE (0.5h) to –0.8439 V vs. SCE (3.5h), then positively to –0.8149 V vs. SCE (15h). The valley potential at 15 h was even higher than the valley potential of the first half hour (0.5h). The increase in the DC valley potential

after 3.5h indicates that the corrosion product starts to inhibit oxygen diffusion to the metal surface after 3.5h [7]. The continued positive shift of the DC valley potential indicates that the corrosion product continues to accumulate at the metal surface.

Figure 6b shows the Nyquist plot of electrochemical impedance recorded under a direct current (DC) density of 0.1A/m^2 with IP of 1/10 at different exposure times (0.5h, 1h, 3h, 6h, 12h, 15h). Each curve exhibits a semicircular arc, a signature of charge-transfer-controlled processes at the electrode/electrolyte interface, which reflects the resistance to electron transfer during redox reactions. The semicircle decreased at 3.5h, then increased, indicating the charge-transfer resistance (Rct) became smaller in the first 3.5h, then became bigger. A similar trend was found in the DC potential change (Figure 6a). Both of the testing methods identified a shift point during the corrosion, which demonstrated the starting point of the corrosion product accumulation that inhibited oxygen diffusion.

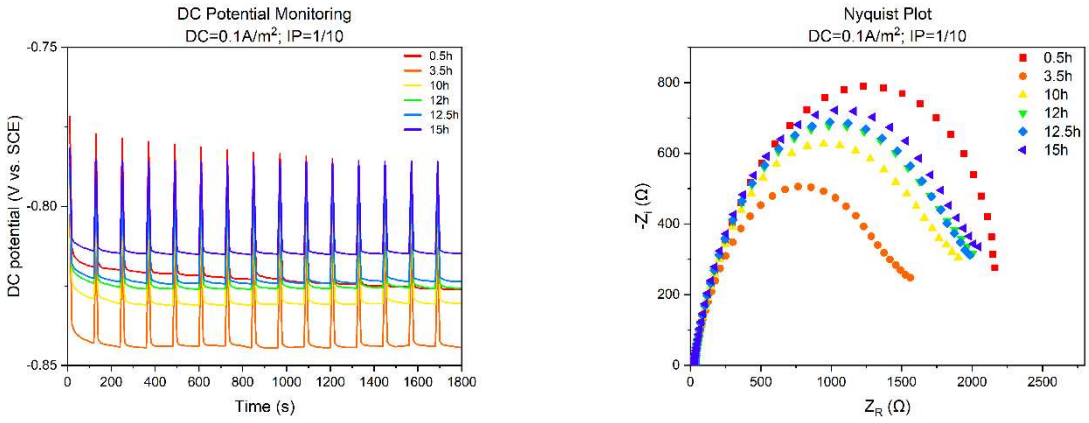

(a) (b)

Figure 6. (a) DC potential monitoring and (b) EIS Nyquist plot of X60 under DC current density of 0.1 A/m^2 and interference period of 1/10 under different time periods.

The DC potential monitoring of X60 steel under DC current density of 1A/m^2 and interference period (IP) of 1/10 under different time periods is shown in Figure 7a. The valley potential gradually shifted negatively from –0.8292 V vs. SCE (0.5h) to –0.8404 V vs. SCE (2h), then positively to –0.8140 V vs. SCE (10h). This shift indicates that the corrosion product continues to accumulate at the metal surface, and the corrosion product starts to inhibit the oxygen diffusion to the metal surface after 2h, which is faster than the X60 under a DC current density of 0.1 A/m^2. This confirms that higher DC current density accelerates the accumulation of the corrosion product.

Figure 7b shows the EIS Nyquist plot of X60 steel under a direct current (DC) density of 1 A/m^2 with IP of 1/10 at different exposure times (0.5h, 2h, 5h, 10h). The semicircle decreased at 2h, then increased, indicating the charge-transfer resistance (Rct) became smaller in the first 2h, then became bigger. Furthermore, this shift point from EIS is consistent with the one identified from DC potential, which confirms that higher DC current density accelerates the corrosion production accumulation.

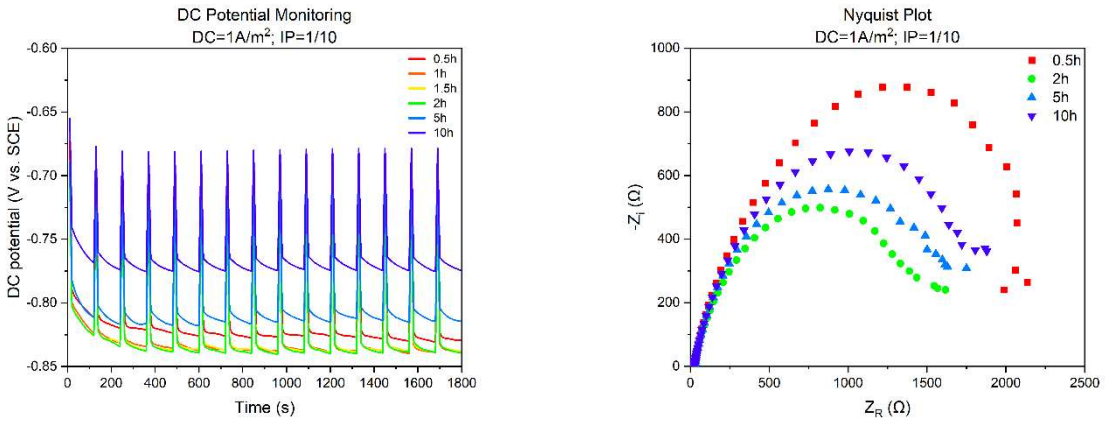

(a) (b)

Figure 7. (a) DC potential monitoring and (b) EIS Nyquist plot of X60 under DC current density of 1 A/m^2 and interference period of 1/10 under different time periods.

3) Tafel testing of X60 under DC interference without CP

Figure 8 shows the Tafel plot for X60 steel under a 1:10 interference period, different DC interference: a) 0.1 A/m^2; b) 1 A/m^2; c) 10 A/m^2, and different durations (1 day and 3 days). The corrosion current and the corrosion potential increased with time.

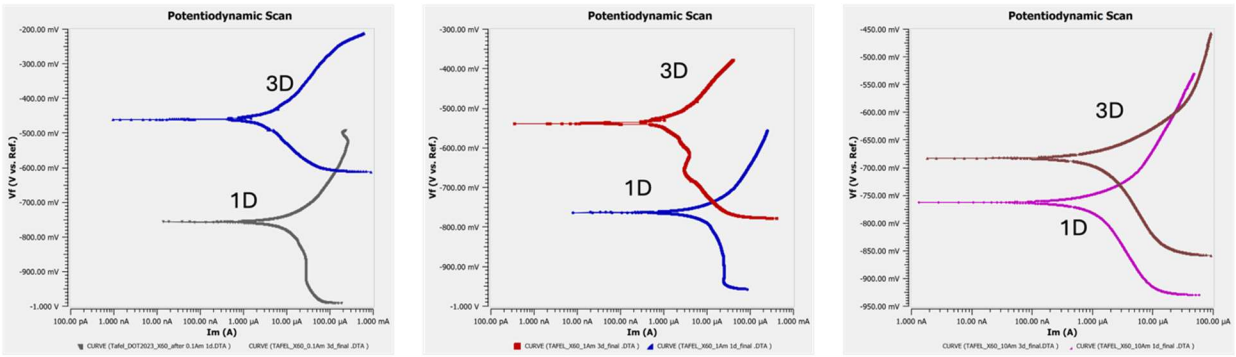

Figure 8. Tafel plot of X60 under DC current density of a) 0.1 A/m^2, b) 1 A/m^2, and c) 10 A/m^2, and interference period of 1/10 under different durations.

Figure 9 shows the surface morphology of X60 under 1/10 interference period, different DC interference, and durations. Under a low current density of 0.1 A/m^2, the surface appeared dark gray, with a uniform and dense texture after 1 day. After 3 days, the surface turned tan, remaining relatively uniform overall. Under a medium current density of 1 A/m^2, the surface became rougher, indicating enhanced reaction activity under the medium current, with reaction products starting to accumulate on the surface after 1 day. After 3 days, yellow spots appeared, with abrupt color changes in local areas. It demonstrates that under long-term medium current, local degradation occurred on the electrode surface. Under a high current density of 10 A/m^2, the surface was mottled with dense holes, and a yellowish corrosion zone appeared at the edge after 1 day. After 3 days, layered corrosion appeared, and it was easy to spall. In conclusion,

the higher the current density and the longer the action time, the more severe the electrochemical damage on the electrode surface.

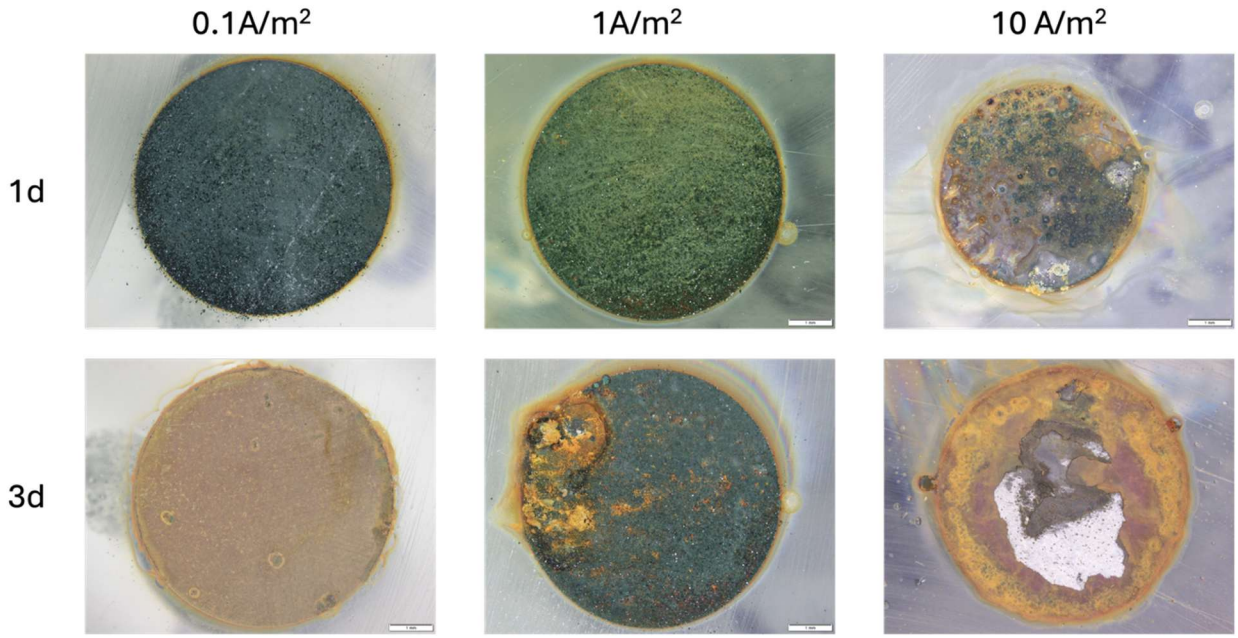

Figure 9. Surface morphology of X60 under different DC current densities and 1/10 interference period with different durations.

3.3. Conclusions

The experimental design and testing protocols for investigating metal corrosion under DC interference with cathodic protection have been established. The corrosion under DC interference with different DC current densities and interference periods has been studied by weight loss measurement and electrochemical characterizations. A systematic study will be continued to know the whole picture of the DC interference corrosion.

4. Task 4 Probabilistic defect growth modeling

4.1. Background and Objectives in the 2nd Annual Report Period

Developing a reliable probabilistic predictive corrosion growth model is critical to estimate time-dependent reliability of a pipeline. Specifically, the explanatory variables (e.g., CP current density, soil properties, coating types, season effect) will be explicitly incorporated, such that the "root cause" of corrosion can be identified.

The corrosion evaluation is modeled through four different responses: corrosion occurrence, corrosion density growth, defect area/volume growth, and defect depth/length growth. This report period focused on the modeling of the first three responses.

4.2. Research Progress in the 2nd Annual Report Period

4.2.1. Prediction modeling on corrosion occurrence on a pipe joint

In this section, the effect of all influencing factors on the occurrence of corrosion on pipe joints are evaluated. Specifically, logistic regression analysis is carried out to develop a predictive model to predict the probability of corrosion occurrence within a pipe joint given the influencing factors. Such a model would help operators better understand and manage their assets and plan future in-line inspections more efficiently.

A subset of available pipe joints is selected where no corrosion was detected on the entire joint in the 1st inspection. These pipe joints are classified into two groups based on whether defects were detected in the 2nd inspection or not. If defects are detected in the 2nd inspection with a joint, the joint is labelled as Class 1, otherwise, it is labelled as Class 0. Therefore, binary logistic regression analysis is used to develop a model which predicts the probability of a pipe joint having corrosion in the next inspection given no corrosion in the 1st ILI. Undersampling technique was utilized so the total number of observations per Class is the same, and balanced dataset is used for model development purposes. Totally, 1,101 observations were used for each Class, results in 2,202 observations for both classes combined. Overall, 22 unique variables were currently used in the developed logistic model, and a detailed investigation on their "importance" and contribution on the accuracy of the model is investigated.

Figure 10 shows the distribution of the predicted probability of having defects in the 2nd inspection obtained from the developed logistic model for two pipelines considered. A perfect model would predict probability values of 1 and 0 for Class 1 and Class 0, respectively. As shown in Figure 10, a clear distinction between the distribution of probabilities for Class 1 and Class 0, i.e., the bule and red distributions, is shown. In particular, the majority of probability values are closer to 1 for Class 1 and the majority of probability values are closer to 0 for Class 0, signifying the good performance of the developed predicted model.

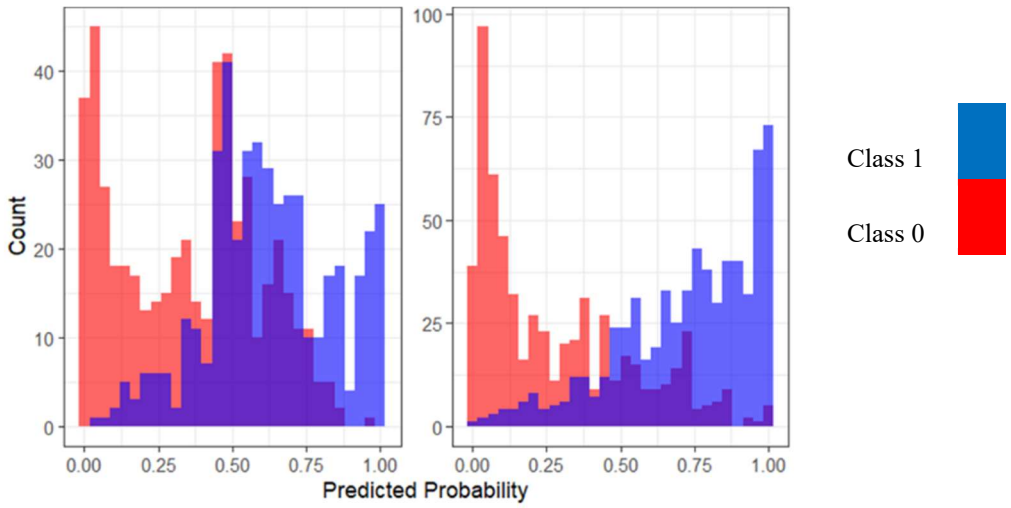

(a) Pipeline 1 (b) Pipeline 2

Figure 10. Predicted probability of having defect in the 2nd inspection

To check if the model prediction is biased (that is, the model is predicting one class with better accuracy than the other), the Root Mean Squared Error (*RMSE*) and Mean Absolute Error (*MAE*) values are calculated using: the ideal probability values, $P_{i,ideal}$ (i.e., $P_{i,ideal} = 0$ and 1 for Class 0 and Class 1 respectively), and the predicted probability values using the developed model, $P_{i,precicted}$, by:

$$RMSE = \sqrt{\frac{1}{n}\sum_{i=1}^{n}(P_{i,predicted} - P_{i,ideal})^2}$$
$$MAE = \frac{1}{n}\sum_{i=1}^{n}\left|P_{i,predicted} - P_{i,ideal}\right| \quad (1)$$

Table 1 summarizes these two performance metrics for each class. As shown, the *RMSE* and *MAE* values are very close for Class 0 and 1, meaning that the model is not predicting the probability values in a biased manner and in favor of one class, and the performance is comparable for both classes.

Table 1. Performance of the logistic regression model considering both classes

Class	Probability *RMSE*	Probability *MAE*
0	0.402	0.314
1	0.388	0.314

The predicted probability values shown in Figure 11 can be assigned to Class 0 and 1 by using a threshold value. A commonly used threshold value for classification is 0.5, as such the probability values in ranges (0, 0.5) and (0.5, 1) being classified as Class 0 and Class 1, respectively. Consequently, the accuracy of the predicted model can be quantified. Figure 11 shows the Receiver Operating Characteristic (ROC) curve for the developed model, which is a graphical representation used to evaluate the performance of a binary classification model. It shows the trade-off between True Positive Rate (TPR) and False Positive Rate (FPR) values at various threshold assumptions. A perfect model would result in an ROC curve passing through the top-left corner, i.e., $TPR = 1$ and $FPR = 0$. The threshold value can be selected subjectively, depending on whether higher *TPR* or lower *FPR* is desirable. For example, three threshold values, *T*, are shown on Figure 11, where threshold of 0.3 results in higher *TPR* and higher *FPR* while a threshold of 0.7 results in lower *TPR* and *FPR*.

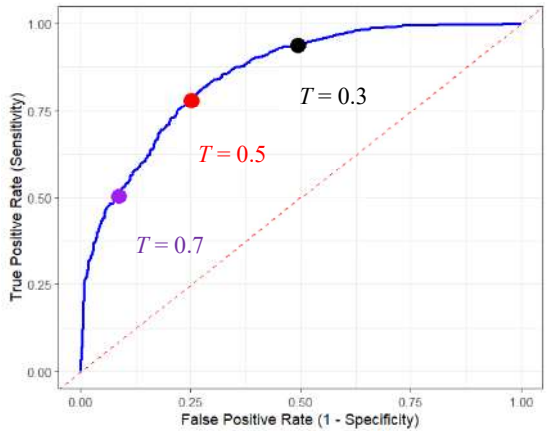

Figure 11. Predicted probability of having defect in the 2nd inspection

The Area Under the Curve (*AUC*) also quantifies the model performance without setting a specific threshold, with a perfect model having $AUC = 1$. Generally, the higher *AUC*, the better the model performance. The *AUC* of this model is calculated to be 0.853 which is considered to be very good, given a balanced (unbiased) dataset of observations is used for model development.

Furthermore, Table 2 summarizes the values of common performance metrics of the developed logistic model, and their definitions are:

$$Accuracy = (TP + TN) / (TP + TN + FP + FN) \tag{2}$$

$$Sensitivity = TPR = TP / (TP + FN) \tag{3}$$

$$Specificity = 1\text{-}\ FPR = TN / (TN + FP) \tag{4}$$

$$Precision = TP / (TP + FP) \tag{5}$$

$$F1 = 2 \times Precision \times Sensitivity / (Precision + Sensitivity) \tag{6}$$

where *TP* = True Positive; *TN* = True Negative; *FP* = False Positive; *FN* = False Negative. In Table 2, these values of these metrics are obtained by applying a threshold value of 0.5 to the prediction model, all of which are above 0.75, implying the good performance of the developed model. In addition, the confusion matrix of the developed model is shown in Table 3, considering the threshold of 0.5. It shows that 77.8% and 74.8% are correctly classified for actual Class 1 and Class 0, respectively.

Table 2. The values of performance metrics of the developed logistic model

Accuracy	TPR	1- FPR	F1
0.76	0.78	0.75	0.77

Table 3. Confusion matrix of the developed logistic model considering threshold of 0.5

		Predicted Class	
		0	1
Actual Class	1	244 (22.2%)	**857 (77.8%)**
	0	**824 (74.8%)**	277 (25.2%)

Test Data Error

As an established assumption in Statistics, cross validation error is considered an unbiased estimate of the error the developed model will have on new, unseen data. Table 4 and 5 summarize respectively the performance metrics and confusion matrix using a 5-fold Cross Validation (CV) technique. In this technique the data is divided into five equal subsets, each subset is used once as the test set while the model is trained on the remaining four, and the results are averaged. As can be seen, the metrics and accuracy are comparable to those mentioned in Tables 2 and 3. Therefore, it is concluded that the developed model is expected to perform on unseen data as well as it does on the training data.

Table 4. The values of performance metrics using 5-fold cross validation

Accuracy	TPR	1-FPR	ROC
0.73	0.81	0.75	0.82

Table 5. Confusion matrix using 5-fold cross validation considering threshold of 0.5

		Predicted Class	
		0	1
Actual Class	1	24.8%	**75.2%**
	0	**70.8%**	29.2%

Importance of variables

Since the model terms include the interaction between variables, SHAP (SHapley Additive exPlanation) values are computed to obtain the contribution of individual variables. For an interaction term (e.g., $x_1 \cdot x_2$), the SHAP framework splits its contribution between x_1 and x_2 based on the covariance between variables x_1 and x_2. Finally, each SHAP value for a variable,

e.g., x_1, is computed as the sum of its average marginal contributions across all interactions it participates in, e.g., $x_1 \cdot x_2$ and $x_1 \cdot x_3$. These SHAP values are obtained and shown in Figure 12 for the variables in the model which highlight the importance of each variable. As can be seen, the *Neighbor_Time* variable which is a constructed variable as the multiplication of *Has Nearby Feature, Time Interval* between ILIs, and *Age at Old ILI* has the highest importance among the considered variables. Note that *Has Nearby Feature* is a binary variable which is zero when the joint adjacent to the joint under study did not have any feature in the old ILI and is equal to one otherwise. Further sensitivity analysis of the model response to the model variables is under study.

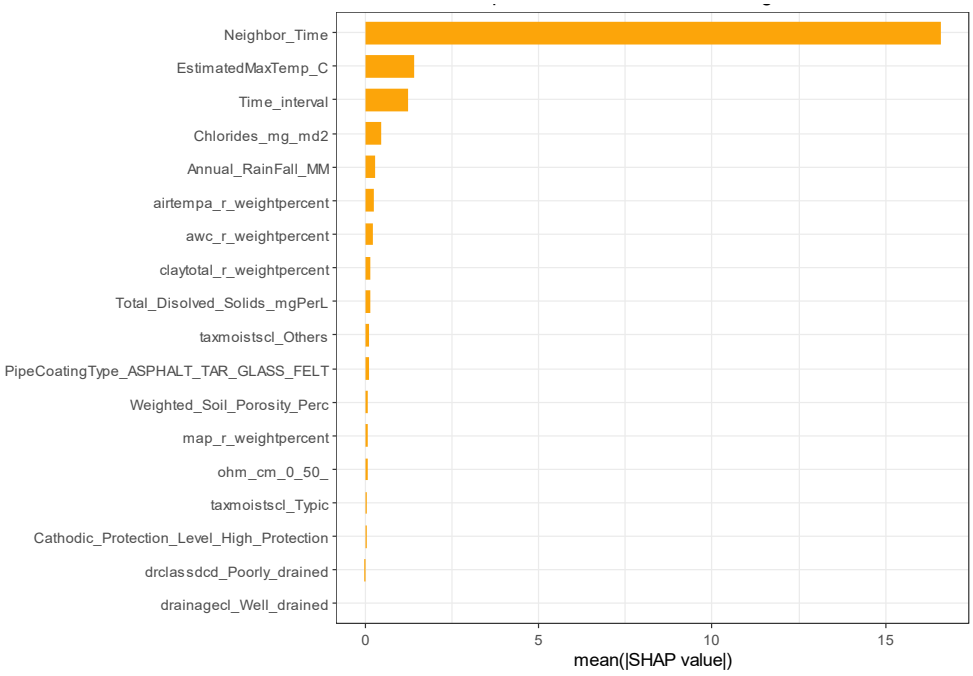

Figure 12. SHAP feature importance with covariance-weighted interactions

4.2.2. Prediction modeling on corrosion density

A time-dependent probabilistic modeling framework has been developed to predict actual external corrosion density in the pipelines using ILI data. The results are compared with a traditional approach of estimating density used by pipeline operators and also with a time-independent model proposed by Stephen and Nessim (2009). An oral presentation was given to present the results in AMPP 2025 Conference in Nashville, TN, in April 2025. This probabilistic modeling framework involves two parameters, λ and t_0. Optimization was performed to estimate these model parameters through Maximum Likelihood method using real data from 4 in-line inspections of two in-service steel pipelines. Overall, 7,939 observations are available.

In this report timeframe, relationship between these two parameters and available environmental and CP variables was investigated in an effort to predict these model parameters using explanatory variables. Two methods were investigated. In Method 1, model parameters

are considered as continuous responses; in Method 2, model parameters are treated as categorical response in which the goal is to predict the levels of parameters, for example to predict whether λ is *High* or *Low* using classification algorithms.

Method 1: model parameter as continuous response

It was found that when the model parameters are considered as continuous responses there is no strong correlation between the response and predictors, leading to poor performance accuracy. A linear regression was performed considering the interaction between variables, and also other advanced machine learning (ML) algorithms, including Gaussian Process Regression and Neural Network, were investigated. To estimate the test data error, CV (Cross Validation) approach was implemented. Although advanced ML models generally provide high prediction accuracy for the training data, their performance significantly reduce when it comes to test data error, because of overfitting. Table 6 summarizes the performance metric for the linear regression model and the advanced model with the best performance in terms of 5-fold CV R^2. As shown, there is not strong relationship between the continuous responses and available predictors. Also, it was observed that the performance of advanced models is not significantly better than Linear Regression model when considering the test data error.

Table 6. Performance metrics of developed models with model parameters as continuous responses

Continuous Response	Linear regression R^2	Best advanced model 5-CV R^2
λ	0.076	0.084
t_0	0.041	0.181

Method 2: model parameter as categorical response

In this method, the model parameter λ is classified into two levels (i.e., High or Low) considering a threshold value. Thus, the model is developed to predict given a set of explanatory variables whether λ is High or Low. This could help pipeline operators to prioritize the inspection of joints where the corrosion density growth rate (λ) is High. Considering a typical joint pipe length is 40 ft, the threshold value considered is the density growth of 1 defect per 40 ft of joint per year.

Figure 23 show the growth of density (i.e., number of defects per pipe joint length) predicted by the optimization framework developed in this research for selected pipe joints. The black line refers to the threshold value density growth rate of 1 defect/40 ft/year, which classifies the growth rates into two separate classes and therefore is used herein. Totally, 2,901 observations were used for each Class, results in 5,802 observations for both classes combined. A binary logistic regression is performed to predict the actual class, i.e., High or Low, of density growth using explanatory variables.

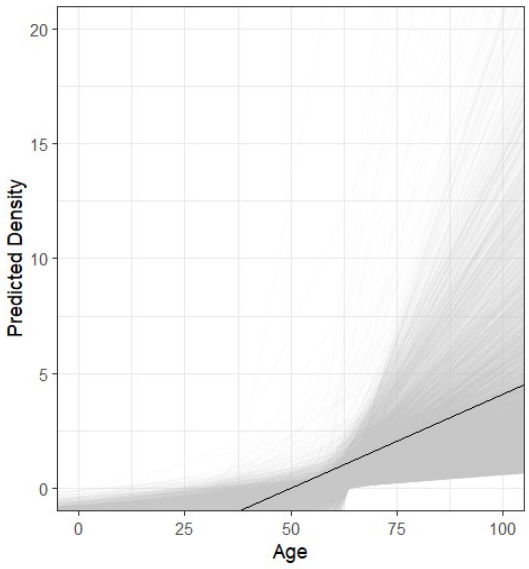

Figure 23 Density growth over time for selected pipe joints

Figure 14 shows the distribution of the predicted probability of having High density growth obtained from the developed logistic model for pipe joints considered. A perfect model would predict probability values of 1 and 0 for Class High and Class Low, respectively. As shown in Figure 14, a clear distinction between the distribution of probabilities for Class High and Class Low, i.e., the bule and red distributions, is shown. In particular, the majority of probability values are closer to 1 for Class High and the majority of probability values are closer to 0 for Class Low, signifying decent performance of the developed predicted model.

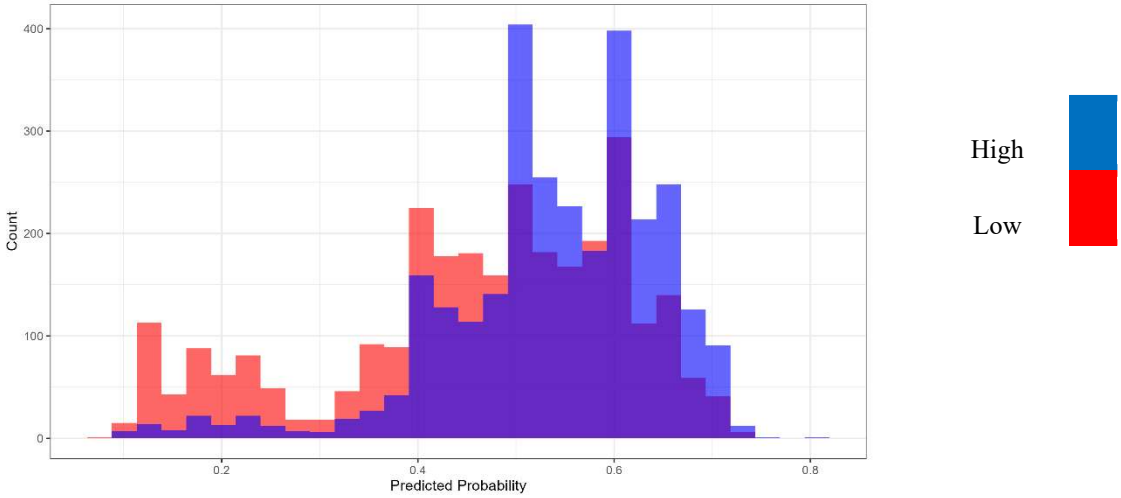

Figure 14 Predicted probability of having High density growth

The predicted probability values shown in Figure 14 can be assigned to Class Low and High by using a threshold value. A commonly used threshold value for classification is 0.5, as such

the calculated probability values in ranges (0, 0.5) and (0.5, 1) are classified as Class Low and Class High, respectively. Consequently, the accuracy of the predicted model can be quantified. Figure 15 shows the Receiver Operating Characteristic (ROC) curve for the developed model, which is a graphical representation used to evaluate the performance of a binary classification model. It shows the trade-off between True Positive Rate (TPR) and False Positive Rate (FPR) values at various threshold assumptions. A perfect model would result in an ROC curve passing through the top-left corner, i.e., $TPR = 1$ and $FPR = 0$. The threshold value can be selected subjectively, depending on whether higher *TPR* or lower *FPR* is desirable. For example, three threshold values, T, are shown on Figure 15, where threshold of 0.3 results in higher *TPR* and higher *FPR* while a threshold of 0.7 results in lower *TPR* and *FPR*.

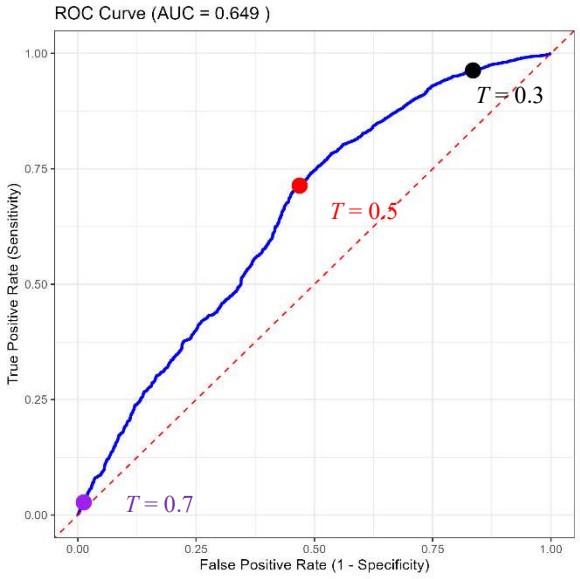

Figure 15 Predicted probability of having High density growth

The Area Under the Curve (*AUC*) also quantifies the model performance without setting a specific threshold, with a perfect model having $AUC = 1$. Generally, the higher *AUC*, the better the model performance. The *AUC* of this model is calculated to be 0.649 which is considered to be acceptable, given a balanced (unbiased) dataset of observations is used for the model development.

In addition to binary classification, a three-level classification and other advanced ML classification models were developed to compare with the performance of the binary classification developed earlier. Five-fold cross validation accuracy is used as the performance metric and Table 7 summarizes these values for the developed binary logistic regression, the best advanced model considering 2 and 3 classes. Although multi-level logistic regression and advanced algorithms might have higher accuracy when training data is concerned, their performance, as shown in Table 7, is not higher than binary logistic regression because they tend to overfit the model based on training data.

Table 7 Performance metrics of developed models with model parameters as categorical responses

Categorical Response	Developed Logistic Regression CV Accuracy	Best advanced ML model CV Accuracy
λ (2 Classes: High or Low)	61%	63%
λ (3 Classes: High or Medium or Low)	-	45%

4.2.3. Corrosion surface area and volume growth

The measurement error of ILI devices and their effect on the calculated external corrosion defect area and volume are considered. According to ILI tool specifications provided by vendors, accuracy of the utilized tools is provided given morphology of an anomaly. For example, depth measurement accuracy is given in terms of 80% confidence interval of x% of the wall thickness. This means that depth measurement is uncertain and there is an 80% chance that the true depth is within the measured depth ±x% of wall thickness. From this information, the uncertainty, i.e., standard deviation, of the measured depth can be obtained by assuming a distribution (e.g., Normal distribution). The measurement error for length or width, however, is usually given in terms of millimeter of the additive sizing error.

The uncertainty in depth, width, and length measurements should be propagated into the calculated area and volume of defects. One could adopt the first-order Taylor expansion to linearize the area and volume functions for simple calculation of the standard deviation of the functions. As an example, Eq. (7) shows the linearization of a function $f(x_1, x_2, x_3)$, using the first-order Taylor expansion around the point a_1, a_2, a_3:

$$f(x_1, x_2, x_3) \approx f(a_1, a_2, a_3) + \sum_{i=1}^{3} \frac{\partial f}{\partial x_i}(a_1, a_2, a_3) \cdot (x_i - a_i) \tag{7}$$

where $\frac{\partial f}{\partial x_i}(a_1, a_2, a_3)$ is the partial derivative of f with respect to x_i evaluated at a_1, a_2, a_3.

To linearize the area function, A, which is the product of width, W, and length, L, using the Taylor series expansion around the mean values of W and L, i.e., μ_W and μ_L, the above equation is used as follows:

$$A = W \cdot L \approx f(\mu_W, \mu_L) + \mu_L (W - \mu_W) + \mu_W (W - \mu_L) \approx \mu_W \cdot L + \mu_L \cdot W - \mu_W \cdot \mu_L \tag{8}$$

Therefore, the mean and standard deviation of area, i.e., μ_A and σ_W, assuming Normal distribution for width and length and independence of W and L, is obtained as follows:

$$\begin{aligned} \mu_A &= \mu_W \cdot \mu_L \\ \sigma_A &= \sqrt{\mu_W{}^2 \cdot \sigma_L{}^2 + \mu_L{}^2 \cdot \sigma_W{}^2} \end{aligned} \tag{9}$$

After estimating the uncertainty of the calculated area (or volume) of defects over different ILIs, the probability of area (or volume) positive growth over time can be estimated using:

$$P\left(Positve\ Growth\right) = P\left(A_2 > A_1\right) = \Phi\left(\frac{\mu_{A_2} - \mu_{A_1}}{\sqrt{\sigma_{A_2}^2 + \sigma_{A_1}^2}}\right) \tag{10}$$

Figure 16 shows the probability that the actual area of defects detected in the second ILI, A_2, of a pipe joint is greater than that in the first ILI, A_1, i.e., *P*(*Postive area growth*), when all the single metal loss (SML) and child features of a pipe joint are considered.

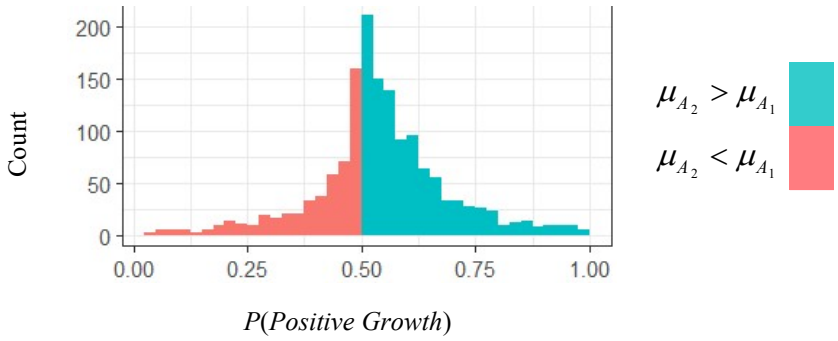

Figure 16. Probability of positive area growth over time

As shown in Figure 16, since Normal distributions are assumed for A_1 and A_2, for the joints where the measured A_2 is greater than the measured A_1, i.e., $\mu_{A_2} > \mu_{A_1}$, *P*(*Positive Growth*) lies in between 0.5 and 1, depending on the A_1 and A_2 distribution parameters. That is, when $\mu_{A_2} > \mu_{A_1}$, the *P*(*Positive Growth*) can sometimes be as low as 0.5, as opposed to the deterministic evaluation with no consideration of measurement errors resulting in 100% of positive growth. On the other hand, when $\mu_{A_2} < \mu_{A_1}$, the *P*(*Positive Growth*) can sometimes be as high as 0.5, while in the deterministic evaluation it would be considered as 100% negative growth. This result shows the importance of considering ILI measurement error and probabilistic evaluation when evaluating the growth of area of defects within a joint over time.

In addition, using the same dataset used in Figure 16, Figure 17 shows for higher values of mean area ratio, i.e., μ_{A_2} / μ_{A_1}, the probability of actual positive area growth over time, i.e., *P*(*Positive Growth*), is generally higher. However, the correlation is not always linear, as it depends on number of defects within a joint, Probability of Detection (POD), and sizing error. It is noted that in theory where $\mu_{A_2} = \mu_{A_1}$, *P*(*Positive Growth*) = 0.5. Moreover, Figure 17 below shows the effect of considering POD on *P*(*Positive Growth*) to be insignificant.

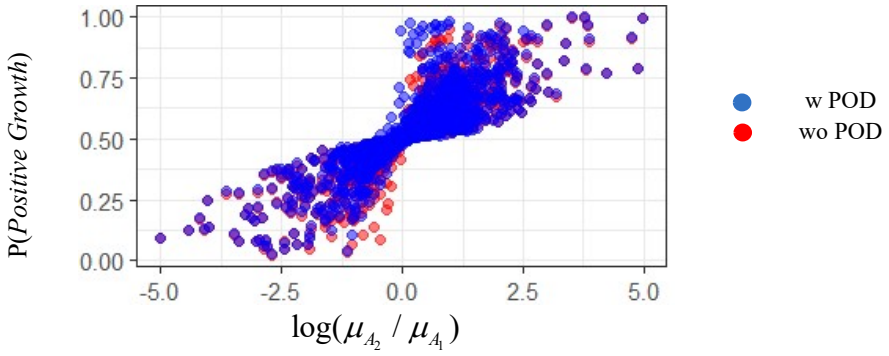

Figure 17. Probability of positive area growth over time versus mean area ratio

4.3. Conclusions

The corrosion evaluation can be described using different quantities. In this task, modeling efforts have been made on predicting probability of corrosion occurrence, corrosion density, and corrosion surface area/volume growth. Using logistic regression, the correlation between probability of corrosion occurrence and explanatory variables is found. The corrosion density is modelled using a passion process considering probability of detection, however, the correlation between the model parameters and the explanatory variables is found to be weak. In addition, the measurement error in the ILI tools are successfully incorporated into the defect surface area/volume growth.

5. Future work

For Task 3, the corrosion of X60 under different DC interference and CP protection will be investigated. A systematic study with different DC current densities and interference periods will be continued by electrochemical characterizations and weight loss measurements.

For Task 4, efforts will be made to investigate possible improvement in the accuracy of the corrosion density model. Sensitivity analysis will be conducted for the developed models for predicting probability of corrosion occurrence and corrosion density. Lastly, probabilistic models will be developed for defect depth and length growth.

References

[1] A. Brenna, P. di Milano, V. Mancinelli, 5721: Effects of Intermittent DC Stray Current on Carbon Steel Under Cathodic Protection, NACE Int. Corros. Conf. Expo (2015).

[2] M. Attarchi, A. Brenna, M. Ormellese, Cathodic protection and DC non-stationary anodic interference, J. Nat. Gas Sci. Eng. 82 (2020) 103497. https://doi.org/10.1016/j.jngse.2020.103497.

[3] S. Qian, Y. Frank Cheng, Corrosion of pipelines under dynamic direct current interference, Constr. Build. Mater. 261 (2020) 120550. https://doi.org/10.1016/j.conbuildmat.2020.120550.

[4] M. Ormellese, S. Beretta, F. Brugnetti, A. Brenna, Effects of non-stationary stray current on carbon steel buried pipelines under cathodic protection, Constr. Build. Mater. 281 (2021) 122645. https://doi.org/10.1016/j.conbuildmat.2021.122645.

[5] H. Qin, Y. Du, M. Lu, Q. Meng, Effect of dynamic DC stray current on corrosion behavior of X70 steel, Mater. Corros. 71 (2020) 35–53. https://doi.org/10.1002/maco.201911022.

[6] H. Qin, T. Zhang, Y. Du, L. Zhang, Y. Zhang, H. Liu, Experimental study of dynamic DC stray current corrosion of X70 steel, Mater. Corros. 74 (2023) 33–52. https://doi.org/10.1002/maco.202213415.

[7] J. Zhang, Z. Li, W. Sun, X. Li, M. Cui, E. Zhou, F. Wang, D. Xu, Extracellular polysaccharides of Tenacibaculum mesophilum D-6 play a major role during its corrosion protection for X80 carbon steel in seawater, Corros. Sci. 249 (2025) 112811. https://doi.org/10.1016/j.corsci.2025.112811.